Journal of Computational Physics **154,** 117–133 (1999)
Article ID jcph.1999.6304, available online at http://www.idealibrary.com on IDEAL®

A Consistent Approach to Large Eddy Simulation Using Adaptive Mesh Refinement[1]

Andrew W. Cook

Lawrence Livermore National Laboratory, Livermore, California 94550
E-mail: awcook@llnl.gov

Received November 5, 1998; revised April 6, 1999

The large eddy simulation of turbulent flows is discussed with particular attention paid to the issue of commutation of differentiation and filtering. Multi-level adaptive mesh refinement is proposed as a means of mostly avoiding commutation errors where increased grid resolution is required to capture key flow features. The strategy is to employ multiple uniform grids in a nested hierarchy using a constant-width filter for each grid. It is shown that commutivity of fine and coarse grid filters must be enforced in order to consistently relate variables at different refinement levels. Methods for treating fine grid boundaries and walls are also discussed. It is shown that errors associated with boundary treatments are small and localized.

Key Words: turbulence; large eddy simulation; adaptive mesh refinement.

1. INTRODUCTION

The Navier–Stokes (N–S) equations in Cartesian coordinates can be written in the following conservation-law form

$$\frac{\partial \mathbf{U}}{\partial t} + \frac{\partial \mathbf{E}}{\partial x} + \frac{\partial \mathbf{F}}{\partial y} + \frac{\partial \mathbf{G}}{\partial z} = 0, \tag{1}$$

where **U**, **E**, **F**, and **G** are suitably defined vectors, representing the mass, momentum, and energy equations [1]. Numerical solutions to the N–S equations typically utilize finite-difference or finite-series approximations to the partial derivatives, such approximations being derived from a truncated Taylor series, polynomial fit, or some other series. At a high enough Reynolds number, the N–S equations admit solutions containing scales of motion that are smaller than the minimum practical grid spacing of any computational mesh. In such cases, discrete approximations to the partial derivatives in (1) will be unrelated to

[1] This work was performed under the auspices of the U.S. Department of Energy by the Lawrence Livermore National Laboratory under Contract W-7405-Eng-48.

0021-9991/99 $30.00

the true derivatives, e.g., the grid spacing may exceed the radius of convergence of Taylor series. Hence, in simulating high Reynolds number flows, only large-scale dynamics can be computed directly, small-scale eddies must be modeled; such calculations are referred to as large eddy simulation (LES).

The first step in performing a LES is to define large-scale variables which can be computed on a given mesh. This theoretical separation of scales is usually accomplished by means of a spatial filter. The filter attenuates high flow frequencies, resulting in a set of variables which can be well-represented on a discrete mesh with wavenumber support up to the Nyquist frequency. Equations governing these large-scale variables are derived by applying the filter to the N–S equations. The resulting "resolved field" or "large eddy" equations differ from the N–S equations in two ways. First, the large-scale variables depend on the filter width, i.e., the volume in space over which the dependent variables have been averaged. The filter width is related to the cell size of the computational mesh. Second, the large eddy equations contain extra subgrid-scale (sgs) terms, which arise when the filter is applied to products in **E**, **F**, and **G**. For example, filtering the advection term in the momentum equation gives rise to the sgs Reynolds stress tensor. The focus of this paper is on the dependence of the large-scale variables on the filter width. This dependence is important when the filter width changes in space and/or time. A change in grid spacing implies a change in filter width, which leads to commutation errors between the filtering and differentiation operations. An example of how grid stretching affects the conservation equations is given in the Appendix.

Several recent works have commented on the errors associated with LES on nonuniform grids and have suggested various strategies for dealing with them. Ghosal and Moin [8] employed a nonlinear mapping procedure to relate a variable-width filter to a given fixed-width filter by using the stretching function of a nonuniform grid. They demonstrated that commutation errors in the filtered N–S equations are second-order and, through spectral analysis, showed that such errors are almost purely dissipative. They also derived higher order corrections that could be used to ensure that the commutation errors do not exceed numerical discretization errors. However, they noted that inclusion of such higher order corrective terms increases the spatial order of the equations so that additional boundary conditions are needed for closure. H. van der Ven [9] derived a set of filters designed to commute with derivatives up to a specified order in the filter width; however, the filters are restricted to unbounded or periodic flows. Fureby and Tabor [7] derived a general expression for errors associated with nonuniform filters which they applied to the N–S equations to formulate the commutation error terms. They evaluated these terms for a channel flow in which the grid spacing was reduced near the walls. They found that, in the wall proximity, the errors were large with respect to advection and were of the order of the viscous contribution in the viscous sublayer. Vasilyev *et al.* [10] suggested the use of explicit filtering for LES, using discrete filtering operators which commute with numerical differentiation to a specified order. With this approach, an extra filtering operation must be performed after each time step and the form of the filter must be tied to the numerical differencing scheme.

The purpose of this work is to discuss how commutation errors can be mostly avoided by employing a multi-level adaptive mesh refinement (AMR) technique, which is summarized in Section 2. In Section 3 a rationale is given for choosing a Gaussian filter, based on its invertibility. In Section 4 a consistency criterion is proposed for relating fine and coarse grid variables. Section 5 describes the treatment of grid boundaries. In Section 6, the matrices which must be inverted for inverse-filtering operations are shown to be well-conditioned.

Section 7 discusses the order of operations to be followed in using data at a given refinement level to compute variables at a different level. In Section 8, errors associated with filtering and inverse-filtering across grid boundaries are quantified. Conclusions are given in Section 9.

2. MULTI-LEVEL REFINEMENT

An optimal LES grid should provide adequate resolution throughout the computational domain without generating excessive commutation errors. In principle, both of these objectives could be achieved using a local adaptive mesh refinement (AMR) technique developed by Berger and Oliger [4], Berger and Collela [3], and Bell *et al.* [2]. The distiguishing feature of this technique is that the data exist at multiple refinement levels in space and time. The flow variables are represented on a nested hierarchy of uniform grids with increasingly finer grids recursively embedded in coarser grids. The meshes are properly nested, such that boundaries of fine grids coincide with grid lines of underlying coarse grids.

An advantage of the multi-level approach to LES is that information on finer grids is available for modeling subgrid-scale terms on coarser grids. Furthermore, the uniformity of the grids allows for the use of a constant-width filter for extracting large-scale variables from the primitive variables; hence, commutation errors are not an issue, except at grid boundaries. In using multiple grids for LES a self-consistent relationship must be established for the flow variables at the various refinement levels. Another problem is how to treat grid boundaries in a manner consistent with a constant-width filter. The remainder of this paper will address these problems.

3. CHOICE OF FILTER

Let fine grid variables be defined by means of an isotropic convolution filter of characteristic width $\bar{\Delta}$, i.e.,

$$\bar{\phi}(\mathbf{x}, t) \equiv \bar{G} * \phi = \int_{\mathbf{R}^3} G(|\mathbf{x} - \mathbf{x}'|/\bar{\Delta})\phi(\mathbf{x}', t)\, d\mathbf{x}', \tag{2}$$

where the integral is over all three-dimensional space (even though the grid may cover only a subdomain of $\mathbf{R}^3$). Similarly, let coarse grid varibles (with characteristic width $\hat{\Delta}$) be defined as

$$\hat{\phi}(\mathbf{x}, t) \equiv \hat{G} * \phi = \int_{\mathbf{R}^3} G(|\mathbf{x} - \mathbf{x}'|/\hat{\Delta})\phi(\mathbf{x}', t)\, d\mathbf{x}'. \tag{3}$$

Assume that ϕ is transformable, e.g., periodic turbulence, with $\mathcal{F}\{\,\}$ denoting a Fourier transform. By the convolution theorem, $\mathcal{F}\{\bar{\phi}\} = \mathcal{F}\{\bar{G}\}\mathcal{F}\{\phi\}$ and $\mathcal{F}\{\hat{\phi}\} = \mathcal{F}\{\hat{G}\}\mathcal{F}\{\phi\}$. Furthermore,

$$\mathcal{F}\{\hat{\bar{\phi}}\} = \mathcal{F}\{\hat{G} * (\bar{G} * \phi)\} = \mathcal{F}\{\hat{G}\}\mathcal{F}\{\bar{G} * \phi\} = \mathcal{F}\{\hat{G}\}\mathcal{F}\{\bar{G}\}\mathcal{F}\{\phi\} = \mathcal{F}\{\bar{\hat{\phi}}\}; \tag{4}$$

therefore, the fine and coarse grid filters commute. If $\mathcal{F}\{G\} \neq 0$ for any wavenumber, then (4) can be used to obtain $\bar{\phi}$, given $\hat{\phi}$, or vice versa; e.g.,

$$\bar{\phi} = \mathcal{F}^{-1}\{\mathcal{F}\{\bar{G}\}\mathcal{F}\{\phi\}\} = \mathcal{F}^{-1}\left\{\frac{\mathcal{F}\{\bar{\hat{\phi}}\}}{\mathcal{F}\{\hat{G}\}}\right\},$$

$$\hat{\phi} = \mathcal{F}^{-1}\{\mathcal{F}\{\hat{G}\}\mathcal{F}\{\phi\}\} = \mathcal{F}^{-1}\left\{\frac{\mathcal{F}\{\hat{\bar{\phi}}\}}{\mathcal{F}\{G\}}\right\}.$$

A logical choice then for the filter kernel is the Gaussian,

$$G = \prod_{i=1}^{3} \frac{1}{\Delta}\sqrt{\frac{6}{\pi}} \exp\left[-6(x_i - x_i')^2/\Delta^2\right], \tag{5}$$

since its transfer function is positive definite, i.e.,

$$\mathcal{F}\{G\} = \int_{-\infty}^{\infty} G(r/\Delta)\exp(-i\kappa r)\, dr = \exp[-(\kappa\Delta)^2/24]\,, \tag{6}$$

where $r = |\mathbf{x} - \mathbf{x}'|$ and κ is the magnitude of the wavevector. The numerical factors in (5) are such that $\int_{-\infty}^{\infty} G(r/\Delta)\, dr = 1$, with the second moment of G being the same as that of a "top-hat" filter of width Δ.

The Nyquist frequency for a computational mesh with grid spacing h is $\kappa_c = \pi/h$ *radians per unit length*. Energy above the Nyquist frequency which is not removed by the filter will be aliased to lower wavenumbers by the discrete sampling of the grid. Therefore, it is desirable to choose a filter-to-grid-width ratio $\Gamma \equiv \Delta/h$ which attenuates wavnumbers greater than κ_c as much as possible without removing too much energy from wavenumbers below κ_c. In Fig. 1, $\mathcal{F}\{G\}$ is plotted versus κh for various Γ; the Nyquist frequency is indicated by the vertical line. The plot suggests that by choosing $\Gamma = 3$, aliasing errors can be kept to a minimum.

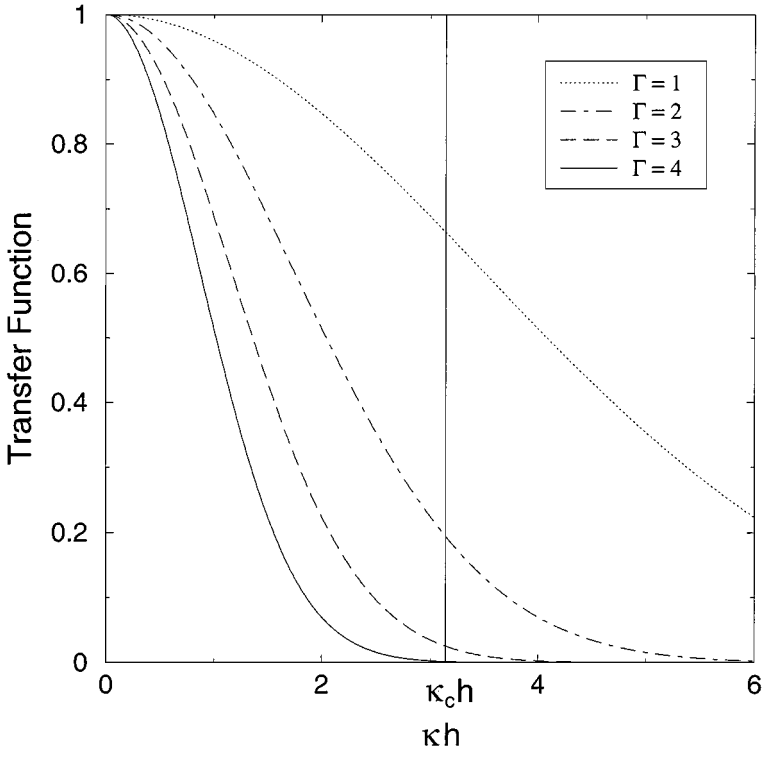

FIG. 1. Transfer function for Gaussian filter with various filter-to-grid-width ratios.

4. CONSISTENCY CRITERION

4.1. *Continuous Case*

A consistency criterion for relating fine and coarse variables is obtained by taking the inverse transform of (4), i.e.,

$$\hat{\bar{\phi}} = \frac{1}{\Gamma^3 \hat{h}^3}\left(\frac{6}{\pi}\right)^{3/2} \int_{\mathbf{R}^3} \exp[-6|\mathbf{x}-\mathbf{x}'|^2/(\Gamma\hat{h})^2]\bar{\phi}(\mathbf{x}', t)\, d\mathbf{x}'$$
$$= \frac{1}{\Gamma^3 \bar{h}^3}\left(\frac{6}{\pi}\right)^{3/2} \int_{\mathbf{R}^3} \exp[-6|\mathbf{x}-\mathbf{x}'|^2/(\Gamma\bar{h})^2]\hat{\phi}(\mathbf{x}', t)\, d\mathbf{x}' = \bar{\hat{\phi}}. \tag{7}$$

For computational convenience, (7) may be split into a series of orthogonal one-dimensional operations, i.e.,

$$\bar{h}\int_{-\infty}^{\infty} \exp[-6(x-x')^2/(\Gamma\hat{h})^2]\alpha(x', y, z, t)\, dx'$$
$$= \hat{h}\int_{-\infty}^{\infty} \exp[-6(x-x')^2/(\Gamma\bar{h})^2]\beta(x', y, z, t)\, dx', \tag{8}$$

where

$$\alpha(x, y, z, t) = \bar{h}\int_{-\infty}^{\infty} \exp[-6(y-y')^2/(\Gamma\hat{h})^2]\theta(x, y', z, t)\, dy', \tag{9}$$

$$\theta(x, y, z, t) = \bar{h}\int_{-\infty}^{\infty} \exp[-6(z-z')^2/(\Gamma\hat{h})^2]\bar{\phi}(x, y, z', t)\, dz', \tag{10}$$

$$\beta(x, y, z, t) = \hat{h}\int_{-\infty}^{\infty} \exp[-6(y-y')^2/(\Gamma\bar{h})^2]\omega(x, y', z, t)\, dy', \tag{11}$$

$$\omega(x, y, z, t) = \hat{h}\int_{-\infty}^{\infty} \exp[-6(z-z')^2/(\Gamma\bar{h})^2]\hat{\phi}(x, y, z', t)\, dz'. \tag{12}$$

4.2. *Discrete Case*

Let i, j, and k be indices of the coarse grid, such that $x = i\hat{h} = \Lambda i\bar{h}$, $y = j\hat{h} = \Lambda j\bar{h}$, and $z = k\hat{h} = \Lambda k\bar{h}$, where $\Lambda \equiv \hat{h}/\bar{h}$ is the grid refinement ratio. Consider the case where $\Lambda = 2$. The first step in discretizing (8)–(12) is to choose stencils of sufficient extent to evaluate the integrals. From a tabulation of the exponentials (see Table I), it is apparent that virtually

TABLE I
Decay of Exponentials for Γ = 3 and Λ = 2

$\lvert i-i'\rvert$	$\exp[-6(i-i')^2/\Gamma^2]$	$\exp[-6\Lambda^2(i-i')^2/\Gamma^2]$
0	1.0	1.0
1	0.5134171190	0.06948345120
2	0.06948345120	$2.330910107 \times 10^{-5}$
3	0.002478752177	$3.775134544 \times 10^{-11}$
4	$2.330910107 \times 10^{-5}$	$2.951903147 \times 10^{-19}$

all of the contributions to the integrals are taken into account by using a seven-point stencil for the integrals involving α, θ, and $\bar{\phi}$, and a three-point stencil for the integrals involving β, ω, and $\hat{\phi}$. The second step in the discretization is to give proper weighting to each of the points in the stencils. This is accomplished by fitting polynomials to the stencils and then evaluating the integrals analytically. The resulting set of discrete equations is (after dividing through by $(\bar{h}\hat{h})^3(3\pi/2)^{3/2}$)

$$\sum_{n=0}^{3} a_n(\alpha_{i-n,j,k} + \alpha_{i+n,j,k}) = \sum_{n=0}^{1} b_n(\beta_{i-n,j,k} + \beta_{i+n,j,k}), \tag{13}$$

$$\alpha_{i,j,k} = \sum_{n=0}^{3} a_n(\theta_{i,j-n,k} + \theta_{i,j+n,k}), \tag{14}$$

$$\theta_{i,j,k} = \sum_{n=0}^{3} a_n(\bar{\phi}_{i,j,k-n} + \bar{\phi}_{i,j,k+n}), \tag{15}$$

$$\beta_{i,j,k} = \sum_{n=0}^{1} b_n(\omega_{i,j-n,k} + \omega_{i,j+n,k}), \tag{16}$$

$$\omega_{i,j,k} = \sum_{n=0}^{1} b_n(\hat{\phi}_{i,j,k-n} + \hat{\phi}_{i,j,k+n}), \tag{17}$$

where

$$a_0 = \frac{353}{1536}, \qquad a_1 = \frac{243}{1024}, \qquad a_2 = \frac{81}{2560}, \qquad a_3 = \frac{19}{15360},$$

$$b_0 = \frac{13}{32}, \qquad b_1 = \frac{3}{32}.$$

This equation set is conservative, i.e., $\sum_{n=0}^{3} a_n = \sum_{n=0}^{1} b_n = 1/2$.

5. BOUNDARY CONDITIONS

5.1. *Internal Grids*

When fine grids are embedded within coarse grids, the fine grid boundaries may be placed at arbitrary locations within the computational domain and may not coincide with physical boundaries. The boundaries of grids embedded in this manner will be referred to as "free" boundaries. Support for filters extending past free boundaries can be provided by extrapolation or one-sided filtering. For example, let the x-boundaries of a fine grid be located at $i = 0$ and $i = I$ and suppose the underlying coarse grid extends past these boundaries. At the nodes, $i = 0, 1, 2, I-2, I-1$, and I, the coarse-grid filter extends beyond the fine grid domain. For these near-boundary nodes, polynomials are constructed using only that portion of the seven-point stencil which lies within the domain of the fine grid. The integral involving α is evaluated using the polynomials based on these subsets of the full stencil. This leads to the conservative

equations

$$\begin{aligned}
\frac{7}{4}\alpha_{0,j,k} - \frac{15}{8}\alpha_{1,j,k} + \frac{3}{2}\alpha_{2,j,k} - \frac{3}{8}\alpha_{3,j,k} &= \psi_{0,j,k}\\
\frac{53}{128}\alpha_{0,j,k} + \frac{3}{32}\alpha_{1,j,k} + \frac{39}{64}\alpha_{2,j,k} - \frac{5}{32}\alpha_{3,j,k} + \frac{5}{128}\alpha_{4,j,k} &= \psi_{1,j,k}\\
\frac{5}{128}\alpha_{0,j,k} + \frac{7}{32}\alpha_{1,j,k} + \frac{31}{64}\alpha_{2,j,k} + \frac{7}{32}\alpha_{3,j,k} + \frac{5}{128}\alpha_{4,j,k} &= \psi_{2,j,k}\\
\lambda_{i,j,k} &= \psi_{i,j,k} \qquad (3 \le i \le I-3)\\
\frac{5}{128}\alpha_{I-4,j,k} + \frac{7}{32}\alpha_{I-3,j,k} + \frac{31}{64}\alpha_{I-2,j,k} + \frac{7}{32}\alpha_{I-1,j,k} + \frac{5}{128}\alpha_{I,j,k} &= \psi_{I-2,j,k}\\
\frac{5}{128}\alpha_{I-4,j,k} - \frac{5}{32}\alpha_{I-3,j,k} + \frac{39}{64}\alpha_{I-2,j,k} + \frac{3}{32}\alpha_{I-1,j,k} + \frac{53}{128}\alpha_{I,j,k} &= \psi_{I-1,j,k}\\
-\frac{3}{8}\alpha_{I-3,j,k} + \frac{3}{2}\alpha_{I-2,j,k} - \frac{15}{8}\alpha_{I-1,j,k} + \frac{7}{4}\alpha_{I,j,k} &= \psi_{I,j,k},
\end{aligned} \tag{18}$$

where

$$\lambda_{i,j,k} = \sum_{n=0}^{3} a_n(\alpha_{i-n,j,k} + \alpha_{i+n,j,k}) \tag{19}$$

and

$$\psi_{i,j,k} = \sum_{n=0}^{1} b_n(\beta_{i-n,j,k} + \beta_{i+n,j,k}). \tag{20}$$

The same procedure can be employed in y and z to close (14) and (15). If the underlying coarse grid extends past all boundaries of the embedded fine grid, then the stencils required for computing ω, β, and ψ are all part of the coarse grid domain.

5.2. *Walls*

For constant-width filters, wall-boundary conditions on filtered variables differ from those of unfiltered variables [7, 10]. This is a consequence of the filters extending beyond the rim of the computational domain. In order to provide support for constant-width filters in the vicinity of walls, assume that the primitive variables can be defined outside the computational domain by extending their boundary values into the wall. To illustrate, suppose a wall is located at $x = x_o (i = 0)$ with $x \ge x_o (i \ge 0)$ being the flow domain. For $x < x_o$, $\bar{\phi}(x, y, z, t)$ and $\hat{\phi}(x, y, z, t)$ asymptote to $\phi(x_o, y, z, t)$. In the discrete case, $\bar{\phi}_{i \le \Gamma/\Lambda, j,k} = \bar{\phi}^{yz}_{0,j,k}$ and $\hat{\phi}_{i \le \Gamma, j,k} = \hat{\phi}^{yz}_{0,j,k}$, where $\bar{\phi}^{yz}_{0,j,k}$ and $\hat{\phi}^{yz}_{0,j,k}$ are the ϕ boundary conditions filtered tangentially to the wall, i.e.,

$$\begin{aligned}
&\bar{\phi}^{yz}(0, y, z, t)\\
&\quad = \frac{6}{\pi\Gamma^2 h^2}\int_{-\infty}^{\infty}\int_{-\infty}^{\infty} \exp\{-6[(y-y')^2 + (z-z')^2]/(\Gamma\bar{h})^2\}\phi(x_o, y', z', t)\, dz'\, dy',\\
&\hat{\phi}^{yz}(0, y, z, t)\\
&\quad = \frac{6}{\pi\Gamma^2 \hat{h}^2}\int_{-\infty}^{\infty}\int_{-\infty}^{\infty} \exp\{-6[(y-y')^2 + (z-z')^2]/(\Gamma\hat{h})^2\}\phi(x_o, y', z', t)\, dz'\, dy'.
\end{aligned}$$

In applying wall-boundary conditions to filtered variables, splines can be used to connect flow-interior solutions to wall-interior boundary conditions. The filtered variables, which

are unknown at $i=-1$, are thus related to known values on either side ($i \le 2$, $i \ge 0$). For example, using $\alpha_{-3/2,j,k} = \bar{\phi}^{yz}_{0,j,k}$, $\alpha_{0,j,k}$, $\alpha_{1,j,k}$, and $\alpha_{2,j,k}$ to construct an interpolating polynomial for $\alpha_{-1,j,k}$, and using $\beta_{-3,j,k} = \hat{\phi}^{yz}_{0,j,k}$, $\beta_{0,j,k}$, and $\beta_{1,j,k}$ to interpolate for $\beta_{-1,j,k}$, leads to

$$\alpha_{-1,j,k} = \frac{16}{35}\bar{\phi}^{yz}_{0,j,k} + \alpha_{0,j,k} - \frac{3}{5}\alpha_{1,j,k} + \frac{1}{7}\alpha_{2,j,k}, \tag{21}$$

$$\beta_{-1,j,k} = \frac{1}{6}\hat{\phi}^{yz}_{0,j,k} + \frac{4}{3}\beta_{0,j,k} - \frac{1}{2}\beta_{1,j,k}. \tag{22}$$

For walls located at $i=0$ and $i=I$, (13) becomes

$$\begin{aligned}
&\frac{15199}{107520}\bar{\phi}^{yz}_{0,j,k} + \frac{2141}{3072}\alpha_{0,j,k} + \frac{243}{2560}\alpha_{1,j,k} + \frac{2349}{35840}\alpha_{2,j,k} + \frac{19}{15360}\alpha_{3,j,k} \\
&\quad = \frac{1}{64}\hat{\phi}^{yz}_{0,j,k} + \frac{15}{16}\beta_{0,j,k} + \frac{3}{64}\beta_{1,j,k} \\
&\frac{8441}{537600}\bar{\phi}^{yz}_{0,j,k} + \frac{1377}{5120}\alpha_{0,j,k} + \frac{16921}{38400}\alpha_{1,j,k} + \frac{8667}{35840}\alpha_{2,j,k} + \frac{81}{2560}\alpha_{3,j,k} \\
&\quad + \frac{19}{15360}\alpha_{4,j,k} = \psi_{1,j,k} \\
&\frac{19}{33600}\bar{\phi}^{yz}_{0,j,k} + \frac{101}{3072}\alpha_{0,j,k} + \frac{757}{3200}\alpha_{1,j,k} + \frac{49439}{107520}\alpha_{2,j,k} + \frac{243}{1024}\alpha_{3,j,k} \\
&\quad + \frac{81}{2560}\alpha_{4,j,k} + \frac{19}{15360}\alpha_{5,j,k} = \psi_{2,j,k} \\
&\qquad\qquad \lambda_{i,j,k} = \psi_{i,j,k} \qquad (3 \le i \le I-3) \qquad (23) \\
&\frac{19}{15360}\alpha_{I-5,j,k} + \frac{81}{2560}\alpha_{I-4,j,k} + \frac{243}{1024}\alpha_{I-3,j,k} + \frac{49439}{107520}\alpha_{I-2,j,k} \\
&\quad + \frac{757}{3200}\alpha_{I-1,j,k} + \frac{101}{3072}\alpha_{I,j,k} + \frac{19}{33600}\bar{\phi}^{yz}_{I,j,k} = \psi_{I-2,j,k} \\
&\frac{19}{15360}\alpha_{I-4,j,k} + \frac{81}{2560}\alpha_{I-3,j,k} + \frac{8667}{35840}\alpha_{I-2,j,k} + \frac{16921}{38400}\alpha_{I-1,j,k} \\
&\quad + \frac{1377}{5120}\alpha_{I,j,k} + \frac{8441}{537600}\bar{\phi}^{yz}_{I,j,k} = \psi_{I-1,j,k} \\
&\frac{19}{15360}\alpha_{I-3,j,k} + \frac{2349}{35840}\alpha_{I-2,j,k} + \frac{243}{2560}\alpha_{I-1,j,k} + \frac{2141}{3072}\alpha_{I,j,k} + \frac{15199}{107520}\bar{\phi}^{yz}_{I,j,k} \\
&\quad = \frac{3}{64}\beta_{I-1,j,k} + \frac{15}{16}\beta_{I,j,k} + \frac{1}{64}\hat{\phi}^{yz}_{I,j,k}.
\end{aligned}$$

Similar closures can be applied for walls on other sides of the flow.

6. INVERTIBILITY OF MATRICES

Let the matrix of α, θ, and $\bar{\phi}$ coefficients for cases where the boundary conditions are periodic, free–free, wall–wall, and wall–free be denoted by A_p, A_f, A_w, and A_m,

respectively. Similarly let the matrix of β, ω, and $\hat{\phi}$ coefficients, for the same cases, be denoted by B_p, B_f, B_w, and B_m. These matrices are given for a seven point grid:

$$A_p = \begin{bmatrix} \frac{353}{768} & \frac{243}{1024} & \frac{81}{2560} & \frac{19}{15360} & \frac{19}{15360} & \frac{81}{2560} & \frac{243}{1024} \\ \frac{243}{1024} & \frac{353}{768} & \frac{243}{1024} & \frac{81}{2560} & \frac{19}{15360} & \frac{19}{15360} & \frac{81}{2560} \\ \frac{81}{2560} & \frac{243}{1024} & \frac{353}{768} & \frac{243}{1024} & \frac{81}{2560} & \frac{19}{15360} & \frac{19}{15360} \\ \frac{19}{15360} & \frac{81}{2560} & \frac{243}{1024} & \frac{353}{768} & \frac{243}{1024} & \frac{81}{2560} & \frac{19}{15360} \\ \frac{19}{15360} & \frac{19}{15360} & \frac{81}{2560} & \frac{243}{1024} & \frac{353}{768} & \frac{243}{1024} & \frac{81}{2560} \\ \frac{81}{2560} & \frac{19}{15360} & \frac{19}{15360} & \frac{81}{2560} & \frac{243}{1024} & \frac{353}{768} & \frac{243}{1024} \\ \frac{243}{1024} & \frac{81}{2560} & \frac{19}{15360} & \frac{19}{15360} & \frac{81}{2560} & \frac{243}{1024} & \frac{353}{768} \end{bmatrix},$$

$$A_f = \begin{bmatrix} \frac{7}{4} & -\frac{15}{8} & \frac{3}{2} & -\frac{3}{8} & 0 & 0 & 0 \\ \frac{53}{128} & \frac{3}{32} & \frac{39}{64} & -\frac{5}{32} & \frac{5}{128} & 0 & 0 \\ \frac{5}{128} & \frac{7}{32} & \frac{31}{64} & \frac{7}{32} & \frac{5}{128} & 0 & 0 \\ \frac{19}{15360} & \frac{81}{2560} & \frac{243}{1024} & \frac{353}{768} & \frac{243}{1024} & \frac{81}{2560} & \frac{19}{15360} \\ 0 & 0 & \frac{5}{128} & \frac{7}{32} & \frac{31}{64} & \frac{7}{32} & \frac{5}{128} \\ 0 & 0 & \frac{5}{128} & -\frac{5}{32} & \frac{39}{64} & \frac{3}{32} & \frac{53}{128} \\ 0 & 0 & 0 & -\frac{3}{8} & \frac{3}{2} & -\frac{15}{8} & \frac{7}{4} \end{bmatrix},$$

$$A_w = \begin{bmatrix} \frac{2141}{3072} & \frac{243}{2560} & \frac{2349}{35840} & \frac{19}{15360} & 0 & 0 & 0 \\ \frac{1377}{5120} & \frac{16921}{38400} & \frac{8667}{35840} & \frac{81}{2560} & \frac{19}{15360} & 0 & 0 \\ \frac{101}{3072} & \frac{757}{3200} & \frac{49439}{107520} & \frac{243}{1024} & \frac{81}{2560} & \frac{19}{15360} & 0 \\ \frac{19}{15360} & \frac{81}{2560} & \frac{243}{1024} & \frac{353}{768} & \frac{243}{1024} & \frac{81}{2560} & \frac{19}{15360} \\ 0 & \frac{19}{15360} & \frac{81}{2560} & \frac{243}{1024} & \frac{49439}{107520} & \frac{757}{3200} & \frac{101}{3072} \\ 0 & 0 & \frac{19}{15360} & \frac{81}{2560} & \frac{8667}{35840} & \frac{16921}{38400} & \frac{1377}{5120} \\ 0 & 0 & 0 & \frac{19}{15360} & \frac{2349}{35840} & \frac{243}{2560} & \frac{2141}{3072} \end{bmatrix},$$

$$A_m = \begin{bmatrix} \frac{2141}{3072} & \frac{243}{2560} & \frac{2349}{35840} & \frac{19}{15360} & 0 & 0 & 0 \\ \frac{1377}{5120} & \frac{16921}{38400} & \frac{8667}{35840} & \frac{81}{2560} & \frac{19}{15360} & 0 & 0 \\ \frac{101}{3072} & \frac{757}{3200} & \frac{49439}{107520} & \frac{243}{1024} & \frac{81}{2560} & \frac{19}{15360} & 0 \\ \frac{19}{15360} & \frac{81}{2560} & \frac{243}{1024} & \frac{353}{768} & \frac{243}{1024} & \frac{81}{2560} & \frac{19}{15360} \\ 0 & 0 & \frac{5}{128} & \frac{7}{32} & \frac{31}{64} & \frac{7}{32} & \frac{5}{128} \\ 0 & 0 & \frac{5}{128} & -\frac{5}{32} & \frac{39}{64} & \frac{3}{32} & \frac{53}{128} \\ 0 & 0 & 0 & -\frac{3}{8} & \frac{3}{2} & -\frac{15}{8} & \frac{7}{4} \end{bmatrix},$$

$$B_p = \frac{1}{32}\begin{bmatrix} 26 & 3 & 0 & 0 & 0 & 0 & 3 \\ 3 & 26 & 3 & 0 & 0 & 0 & 0 \\ 0 & 3 & 26 & 3 & 0 & 0 & 0 \\ 0 & 0 & 3 & 26 & 3 & 0 & 0 \\ 0 & 0 & 0 & 3 & 26 & 3 & 0 \\ 0 & 0 & 0 & 0 & 3 & 26 & 3 \\ 3 & 0 & 0 & 0 & 0 & 3 & 26 \end{bmatrix}, \qquad B_f = \frac{1}{32}\begin{bmatrix} 26 & 3 & 0 & 0 & 0 & 0 & 0 \\ 3 & 26 & 3 & 0 & 0 & 0 & 0 \\ 0 & 3 & 26 & 3 & 0 & 0 & 0 \\ 0 & 0 & 3 & 26 & 3 & 0 & 0 \\ 0 & 0 & 0 & 3 & 26 & 3 & 0 \\ 0 & 0 & 0 & 0 & 3 & 26 & 3 \\ 0 & 0 & 0 & 0 & 0 & 3 & 26 \end{bmatrix},$$

$$B_w = \frac{1}{64}\begin{bmatrix} 60 & 3 & 0 & 0 & 0 & 0 & 0 \\ 6 & 52 & 6 & 0 & 0 & 0 & 0 \\ 0 & 6 & 52 & 6 & 0 & 0 & 0 \\ 0 & 0 & 6 & 52 & 6 & 0 & 0 \\ 0 & 0 & 0 & 6 & 52 & 6 & 0 \\ 0 & 0 & 0 & 0 & 6 & 52 & 6 \\ 0 & 0 & 0 & 0 & 0 & 3 & 60 \end{bmatrix}, \qquad B_m = \frac{1}{64}\begin{bmatrix} 60 & 3 & 0 & 0 & 0 & 0 & 0 \\ 6 & 52 & 6 & 0 & 0 & 0 & 0 \\ 0 & 6 & 52 & 6 & 0 & 0 & 0 \\ 0 & 0 & 6 & 52 & 6 & 0 & 0 \\ 0 & 0 & 0 & 6 & 52 & 6 & 0 \\ 0 & 0 & 0 & 0 & 6 & 52 & 6 \\ 0 & 0 & 0 & 0 & 0 & 6 & 52 \end{bmatrix}.$$

The B matrices are all diagonally dominant, and hence, invertible. The A matrices are not diagonally dominant; however, they are all well-conditioned, i.e., $\text{cond}(A_p) = 16.85$, $\text{cond}(A_f) = 202.7$, $\text{cond}(A_w) = 15.48$, and $\text{cond}(A_m) = 182.6$; hence, the A matrices are also invertible.

7. METHODOLOGY

7.1. *Using Coarse Grid Data to Initialize Fine Grids*

The procedure for computing variables at a particular refinement level from variables at another level involves a filtering step and an inversion step. The process is outlined as $\hat{\phi} \leftrightarrow \hat{\bar{\phi}} = \bar{\hat{\phi}} \leftrightarrow \bar{\phi}$, where the computation may proceed in either direction.

The first step in computing $\bar{\phi}$ from $\hat{\phi}$ is to calculate ω, β, and ψ using (17), (16), and (20); closures such as (22) are used where walls are present. The second step is to combine (13), (14), and (15) with the appropriate boundary conditions and invert the system on the coarse grid to obtain α, θ, and ϕ. The third step is to interpolate $\bar{\phi}$ onto the fine grid. Interpolation will, in general, introduce wavenumbers above the Nyquist frequency of the coarse grid (i.e., in the range $\pi/\hat{\bar{h}} \le \kappa \le \pi/\bar{h}$). These frequencies will probably not be related to the higher frequencies in $\bar{\phi}$, which would remain after filtering the actual function ϕ. Therefore, it is recommended that interpolation onto the fine grid be done after the filter inversion, rather than before, to avoid amplification of numerically generated wavenumbers. The rationale here is similar to the reasoning behind the subgrid-scale estimation model of Domaradzki and Loh [5]. In their model, a deconvolution is performed to amplify wavenumbers just below the grid-scale cutoff, then a nonlinear operation is applied to the deconvolved field, which generates higher frequencies for the estimated variable [6]. Such a model may be a natural choice for an AMR calculation, since the deconvolution, used to initialize fine grids,

may also be used for subgrid-scale modeling on the finest grid. Subgrid-scale models on coarser grids could be constructed by filtering products on embedded fine grids.

7.2. *Using Fine Grid Data to Correct Coarse Grid Data*

The first step in computing $\hat{\phi}$ from $\bar{\phi}$ is to use (15), (14), and (19), in succession, to compute $\theta_{i,j,k}$, $\alpha_{i,j,k}$, and $\lambda_{i,j,k}$ at nodes where the filter stencils are entirely contained within the domain of the fine grid. For the remaining nodes, pre-corrected values for $\hat{\phi}$ are used in (17), (16), and (20) to compute $\omega_{i,j,k}$, $\beta_{i,j,k}$, and $\psi_{i,j,k} = \lambda_{i,j,k}$. The second step is to combine (13), (16), and (17) with the appropriate boundary conditions and invert each set, in succession to obtain $\beta_{i,j,k}$, $\omega_{i,j,k}$, and $\hat{\bar{\phi}}_{i,j,k}$. In performing the inversions, the off-boundary and/or wall-boundary elements are moved to the left-hand side of the equations. This procedure ensures that the corrected solution will blend smoothly with the pre-corrected solution across fine grid boundaries.

8. ERROR ANALYSIS

Because the filter stencils change near grid boundaries, some errors can occur in these regions. In order to quantify errors associated with free boundaries, fine and coarse grid filters were applied to sine waves of different wavelengths. The coarse grid representation of each wave ($\hat{\phi}$) was then used to reconstruct $\bar{\phi}$ on a fine grid embedded within the coarse grid. Figure 2 shows the results of this exercise. The agreement between the reconstructed

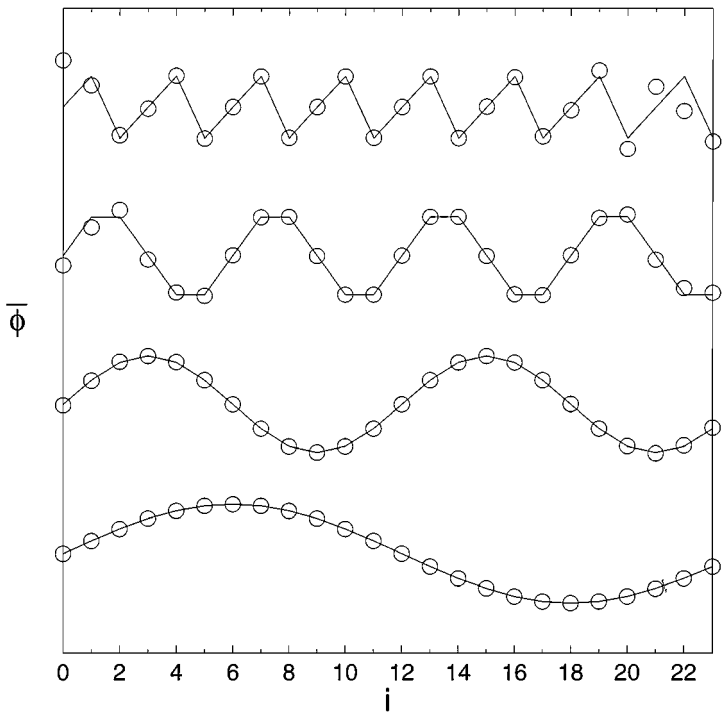

FIG. 2. Fine-grid representations of various Fourier modes. The boundaries of the fine grid are located at $i = 0$ and $i = 23$. The solid lines are the result of filtering ϕ; the circles are the result of inverting $\hat{\phi}$.

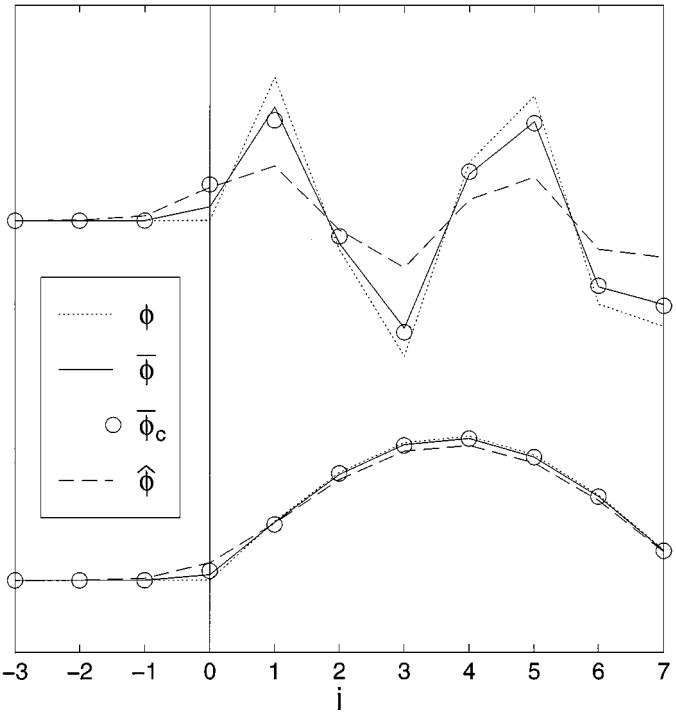

FIG. 3. Fine- and coarse-grid functions near a wall, located at $i = 0$. The true fine-grid solution $\bar{\phi}$ was obtained by filtering ϕ, whereas $\bar{\phi}_c$ was obtained by inverting $\hat{\phi}$.

functions (circles) and the true functions (lines) is excellent. The errors are localized near the boundaries and are only significant for modes close to the Nyquist frequency.

Results of filtering near a wall boundary are displayed in Fig. 3. Here $\bar{\phi}$ and $\hat{\phi}$ result from filtering ϕ with the fine and coarse grid filters, respectively. The computed solution $\bar{\phi}_c$ is obtained by inverting $\hat{\phi}$. Once again, the agreement between $\bar{\phi}$ and $\bar{\phi}_c$ is very good except in the high frequency case at the wall boundary.

9. CONCLUSIONS

By using multiple uniform grids (as opposed to grid stretching) to meet local resolution requirements, a single filter of constant width can be defined for each grid, thus ensuring commutivity of filtering and differentiation. This approach, however, introduces some new problems; namely, how to relate variables on embedded fine grids to variables on underlying coarse grids and how to provide support for filters near grid boundaries.

Consistency between fine and coarse grid variables can be ensured by enforcing commutivity of fine and coarse grid filters. A method has been presented for computing a fine grid solution given a coarse grid solution and vice versa. The procedure involves a filtering step, to compute an intermediate quantity, followed by a deconvolution to obtain the function at a different refinement level. A Gaussian filter is used, because its transfer function has no zero crossings in wavenumber space, and hence, it is invertible.

In treating embedded grids, some errors occur near grid boundaries as a result of changing the filter stencil in these regions. The errors are local and are very small unless high

wavenumber modes are present. If wavenumbers close to the Nyquist frequency are damped by a subgrid-scale model, then it may be possible to place fine grids within turbulent flow regions without generating significant boundary errors. However, shocks, material-interfaces, and other high-frequency phenomena should not be allowed to cross grid boundaries.

Wall-boundary conditions on filtered variables can be supplied by applying boundary values for the corresponding primitive variables at a distance of one filter width into the wall. This scheme is consistent with the use of a constant-width filter; however, it is subject to interpolation error, since the flow at the wall must be matched to the boundary conditions applied inside the wall. These errors have been shown to be very small and highly localized and are only significant when high frequency modes are in contact with the wall.

APPENDIX

Effect of Grid Stretching on Governing Equations

Assume a Cartesian mesh which may be stretched independently in x, y, z, and t. Let large-scale variables be defined as grid-cell averages of the primitive variables, i.e.,

$$\bar{\phi}(x, y, z, t) \equiv \frac{1}{h_x h_y h_z} \int_{x-h_x/2}^{x+h_x/2} \int_{y-h_y/2}^{y+h_y/2} \int_{z-h_z/2}^{z+h_z/2} \phi(x', y', z', t)\, dz'\, dy'\, dx', \quad \text{(A.1)}$$

where ϕ is any variable, $\bar{\phi}$ is its large-scale component, and $h_x(x, y, z, t)$, $h_y(x, y, z, t)$, and $h_z(x, y, z, t)$ are the grid spacings.

Applying (A.1) to $\partial \mathbf{U}/\partial t$, and using Leibnitz's rule, results in

$$\begin{aligned}
\overline{\frac{\partial \mathbf{U}}{\partial t}} &= \frac{1}{h_x h_y h_z} \int_{x-h_x/2}^{x+h_x/2} \int_{y-h_y/2}^{y+h_y/2} \int_{z-h_z/2}^{z+h_z/2} \frac{\partial \mathbf{U}(x', y', z', t)}{\partial t}\, dz'\, dy'\, dx' \\
&= \frac{1}{h_x h_y h_z} \int_{x-h_x/2}^{x+h_x/2} \int_{y-h_y/2}^{y+h_y/2} \left\{ \frac{\partial}{\partial t} \int_{z-h_z/2}^{z+h_z/2} \mathbf{U}(x', y', z', t)\, dz' \right. \\
&\quad \left. - \left[\frac{\partial h_z(x, y, z, t)}{\partial t} \right] \left[\frac{\mathbf{U}(x', y', z - h_z/2, t) + \mathbf{U}(x', y', z + h_z/2, t)}{2} \right] \right\} dy'\, dx'.
\end{aligned}$$

The last term is the trapezoidal formula for definite integrals. Application of the trapezoidal rule in reverse (including error) gives

$$\begin{aligned}
\overline{\frac{\partial \mathbf{U}}{\partial t}} &= \frac{1}{h_x h_y h_z} \int_{x-h_x/2}^{x+h_x/2} \int_{y-h_y/2}^{y+h_y/2} \left\{ \frac{\partial}{\partial t} \int_{z-h_z/2}^{z+h_z/2} \mathbf{U}(x', y', z', t)\, dz' \right. \\
&\quad \left. - \left[\frac{\partial h_z(x, y, z, t)}{\partial t} \right] \left[\frac{1}{h_z(x, y, z, t)} \right] \left[\int_{z-h_z/2}^{z+h_z/2} \mathbf{U}(x', y', z', t)\, dz' + \mathcal{O}\left(h_z^3\right) \right] \right\} dy'\, dx' \\
&= \frac{1}{h_x h_y h_z} \int_{x-h_x/2}^{x+h_x/2} \int_{y-h_y/2}^{y+h_y/2} \frac{\partial}{\partial t} \int_{z-h_z/2}^{z+h_z/2} \mathbf{U}(x', y', z', t)\, dz'\, dy'\, dx' \\
&\quad - \frac{\partial h_z}{\partial t} \left(\frac{1}{h_z} \right) \bar{\mathbf{U}} - \frac{\partial h_z}{\partial t} \mathcal{O}(h_z).
\end{aligned}$$

Repeating these procedures for the y and x integrals yields

$$\overline{\frac{\partial \mathbf{U}}{\partial t}} = \frac{1}{h_x h_y h_z}\frac{\partial}{\partial t}\int_{x-h_x/2}^{x+h_x/2}\int_{y-h_y/2}^{y+h_y/2}\int_{z-h_z/2}^{z+h_z/2}\mathbf{U}(x',y',z',t)\,dz'\,dy'\,dx' - \left(\frac{\partial h_x}{\partial t}\frac{1}{h_x}+\frac{\partial h_y}{\partial t}\frac{1}{h_y}+\frac{\partial h_z}{\partial t}\frac{1}{h_z}\right)\bar{\mathbf{U}} - \frac{\partial h_x}{\partial t}\mathcal{O}(h_x) - \frac{\partial h_y}{\partial t}\mathcal{O}(h_y) - \frac{\partial h_z}{\partial t}\mathcal{O}(h_z).$$

Applying the product rule to the first term results in

$$\overline{\frac{\partial \mathbf{U}}{\partial t}} = \frac{\partial \bar{\mathbf{U}}}{\partial t} - \frac{\partial}{\partial t}\left(\frac{1}{h_x h_y h_z}\right)\int_{x-h_x/2}^{x+h_x/2}\int_{y-h_y/2}^{y+h_y/2}\int_{z-h_z/2}^{z+h_z/2}\mathbf{U}(x',y',z',t)\,dz'\,dy'\,dx' - \left(\frac{\partial h_x}{\partial t}\frac{1}{h_x}+\frac{\partial h_y}{\partial t}\frac{1}{h_y}+\frac{\partial h_z}{\partial t}\frac{1}{h_z}\right)\bar{\mathbf{U}} - \frac{\partial h_x}{\partial t}\mathcal{O}(h_x) - \frac{\partial h_y}{\partial t}\mathcal{O}(h_y) - \frac{\partial h_z}{\partial t}\mathcal{O}(h_z). \tag{A.2}$$

Now,

$$\begin{aligned}\frac{\partial}{\partial t}\left(\frac{1}{h_x h_y h_z}\right) &= h_x^{-1}h_y^{-1}\frac{\partial h_z^{-1}}{\partial t} + h_x^{-1}h_z^{-1}\frac{\partial h_y^{-1}}{\partial t} + h_y^{-1}h_z^{-1}\frac{\partial h_x^{-1}}{\partial t}\\ &= -\left(\frac{\partial h_x}{\partial t}\frac{1}{h_x}+\frac{\partial h_y}{\partial t}\frac{1}{h_y}+\frac{\partial h_z}{\partial t}\frac{1}{h_z}\right)\frac{1}{h_x h_y h_z};\end{aligned}$$

thus, the terms involving $(\partial h_\xi/\partial t)(1/h_\xi)$ in (A.2) all cancel, and the result is

$$\overline{\frac{\partial \mathbf{U}}{\partial t}} = \frac{\partial \bar{\mathbf{U}}}{\partial t} - \frac{\partial h_x}{\partial t}\mathcal{O}(h_x) - \frac{\partial h_y}{\partial t}\mathcal{O}(h_y) - \frac{\partial h_z}{\partial t}\mathcal{O}(h_z). \tag{A.3}$$

Averaging $\partial \mathbf{E}/\partial x$ yields

$$\begin{aligned}\overline{\frac{\partial \mathbf{E}}{\partial x}} &= \frac{1}{h_x h_y h_z}\int_{z-h_z/2}^{z+h_z/2}\int_{y-h_y/2}^{y+h_y/2}\int_{x-h_x/2}^{x+h_x/2}\frac{\partial \mathbf{E}(x',y',z',t)}{\partial x'}\,dx'\,dy'\,dz'\\ &= \frac{1}{h_x h_y h_z}\int_{z-h_z/2}^{z+h_z/2}\int_{y-h_y/2}^{y+h_y/2}[\mathbf{E}(x+h_x/2,y',z',t)-\mathbf{E}(x-h_x/2,y',z',t)]\,dy'\,dz'.\end{aligned} \tag{A.4}$$

In order to relate this to $\partial \bar{\mathbf{E}}/\partial x$, consider

$$\begin{aligned}\frac{\partial \bar{\mathbf{E}}}{\partial x} &= \frac{\partial}{\partial x}\left[\frac{1}{h_x h_y h_z}\int_{z-h_z/2}^{z+h_z/2}\int_{y-h_y/2}^{y+h_y/2}\int_{x-h_x/2}^{x+h_x/2}\mathbf{E}(x',y',z',t)\,dx'\,dy'\,dz'\right]\\ &= \frac{\partial}{\partial x}\left(\frac{1}{h_x h_y h_z}\right)\int_{z-h_z/2}^{z+h_z/2}\int_{y-h_y/2}^{y+h_y/2}\int_{x-h_x/2}^{x+h_x/2}\mathbf{E}(x',y',z',t)\,dx'\,dy'\,dz'\\ &\quad + \frac{1}{h_x h_y h_z}\frac{\partial}{\partial x}\int_{z-h_z/2}^{z+h_z/2}\int_{y-h_y/2}^{y+h_y/2}\int_{x-h_x/2}^{x+h_x/2}\mathbf{E}(x',y',z',t)\,dx'\,dy'\,dz'\\ &= -\left(\frac{\partial h_x}{\partial x}\frac{1}{h_x}+\frac{\partial h_y}{\partial x}\frac{1}{h_y}+\frac{\partial h_z}{\partial x}\frac{1}{h_z}\right)\bar{\mathbf{E}}\end{aligned}$$

$$
\begin{aligned}
&+\frac{1}{h_x h_y h_z}\left\{\int_{z-h_z/2}^{z+h_z/2}\frac{\partial}{\partial x}\int_{y-h_y/2}^{y+h_y/2}\int_{x-h_x/2}^{x+h_x/2}\mathbf{E}(x',y',z',t)\,dx'\,dy'\,dz'\right.\\
&\left.+\frac{\partial h_z}{\partial x}\int_{y-h_y/2}^{y+h_y/2}\int_{x-h_x/2}^{x+h_x/2}\frac{1}{2}[\mathbf{E}(x',y',z-h_z/2,t)+\mathbf{E}(x',y',z+h_z/2,t)]\,dx'\,dy'\right\}\\
&=-\left(\frac{\partial h_x}{\partial x}\frac{1}{h_x}+\frac{\partial h_y}{\partial x}\frac{1}{h_y}+\frac{\partial h_z}{\partial x}\frac{1}{h_z}\right)\bar{\mathbf{E}}\\
&\quad+\frac{1}{h_x h_y h_z}\int_{z-h_z/2}^{z+h_z/2}\frac{\partial}{\partial x}\int_{y-h_y/2}^{y+h_y/2}\int_{x-h_x/2}^{x+h_x/2}\mathbf{E}(x',y',z',t)\,dx'\,dy'\,dz'+\frac{\partial h_z}{\partial x}\frac{1}{h_x h_y h_z}\\
&\quad\times\int_{y-h_y/2}^{y+h_y/2}\int_{x-h_x/2}^{x+h_x/2}\frac{1}{h_z(x,y,z,t)}\left[\int_{z-h_z/2}^{z+h_z/2}\mathbf{E}(x',y',z',t)\,dz'+\mathcal{O}\big(h_z^3\big)\right]dx'\,dy'.
\end{aligned}
$$

The second to last term cancels the third term; thus,

$$
\begin{aligned}
\frac{\partial\bar{\mathbf{E}}}{\partial x}&=-\left(\frac{\partial h_x}{\partial x}\frac{1}{h_x}+\frac{\partial h_y}{\partial x}\frac{1}{h_y}\right)\bar{\mathbf{E}}\\
&\quad+\frac{1}{h_x h_y h_z}\int_{z-h_z/2}^{z+h_z/2}\frac{\partial}{\partial x}\int_{y-h_y/2}^{y+h_y/2}\int_{x-h_x/2}^{x+h_x/2}\mathbf{E}(x',y',z',t)\,dx'\,dy'\,dz'+\frac{\partial h_z}{\partial x}\mathcal{O}(h_z).
\end{aligned}
$$

Repeating the above procedure for $\partial/\partial x$ of the y integral yields

$$
\begin{aligned}
\frac{\partial\bar{\mathbf{E}}}{\partial x}&=-\frac{\partial h_x}{\partial x}\frac{1}{h_x}\bar{\mathbf{E}}+\frac{1}{h_x h_y h_z}\int_{z-h_z/2}^{z+h_z/2}\int_{y-h_y/2}^{y+h_y/2}\frac{\partial}{\partial x}\int_{x-h_x/2}^{x+h_x/2}\mathbf{E}(x',y',z',t)\,dx'\,dy'\,dz'\\
&\quad+\frac{\partial h_y}{\partial x}\mathcal{O}(h_y)+\frac{\partial h_z}{\partial x}\mathcal{O}(h_z).
\end{aligned}
$$

Applying Leibnitz's rule to $\partial/\partial x$ of the x integral results in

$$
\begin{aligned}
\frac{\partial\bar{\mathbf{E}}}{\partial x}&=-\frac{\partial h_x}{\partial x}\frac{1}{h_x}\bar{\mathbf{E}}+\frac{1}{h_x h_y h_z}\int_{z-h_z/2}^{z+h_z/2}\int_{y-h_y/2}^{y+h_y/2}\left[\left(1+\frac{1}{2}\frac{\partial h_x(x,y,z,t)}{\partial x}\right)\mathbf{E}(x+h_x/2,y',z',t)\right.\\
&\quad\left.-\left(1-\frac{1}{2}\frac{\partial h_x(x,y,z,t)}{\partial x}\right)\mathbf{E}(x-h_x/2,y',z',t)\right]dy'\,dz'+\frac{\partial h_y}{\partial x}\mathcal{O}(h_y)+\frac{\partial h_z}{\partial x}\mathcal{O}(h_z)\\
&=-\frac{\partial h_x}{\partial x}\frac{1}{h_x}\bar{\mathbf{E}}+\frac{1}{h_x h_y h_z}\int_{z-h_z/2}^{z+h_z/2}\int_{y-h_y/2}^{y+h_y/2}[\mathbf{E}(x+h_x/2,y',z',t)\\
&\quad-\mathbf{E}(x-h_x/2,y',z',t)]\,dy'\,dz'+\frac{1}{h_x h_y h_z}\int_{z-h_z/2}^{z+h_z/2}\int_{y-h_y/2}^{y+h_y/2}\frac{\partial h_x(x,y,z,t)}{\partial x}\\
&\quad\times\frac{1}{2}[\mathbf{E}(x-h_x/2,y',z',t)+\mathbf{E}(x+h_x/2,y',z',t)]\,dy'\,dz'+\frac{\partial h_y}{\partial x}\mathcal{O}(h_y)+\frac{\partial h_z}{\partial x}\mathcal{O}(h_z)\\
&=-\frac{\partial h_x}{\partial x}\frac{1}{h_x}\bar{\mathbf{E}}+\frac{\overline{\partial\mathbf{E}}}{\partial x}+\frac{\partial h_x}{\partial x}\frac{1}{h_x h_y h_z}\int_{z-h_z/2}^{z+h_z/2}\int_{y-h_y/2}^{y+h_y/2}\frac{1}{h_x(x,y,z,t)}\\
&\quad\times\left[\int_{x-h_x/2}^{x+h_x/2}\mathbf{E}(x',y',z',t)\,dx'+\mathcal{O}\big(h_x^3\big)\right]dy'\,dz'+\frac{\partial h_y}{\partial x}\mathcal{O}(h_y)+\frac{\partial h_z}{\partial x}\mathcal{O}(h_z).
\end{aligned}
$$

Therefore,

$$\overline{\frac{\partial \mathbf{E}}{\partial x}} = \frac{\partial \bar{\mathbf{E}}}{\partial x} - \frac{\partial h_x}{\partial x}\mathcal{O}(h_x) - \frac{\partial h_y}{\partial x}\mathcal{O}(h_y) - \frac{\partial h_z}{\partial x}\mathcal{O}(h_z). \tag{A.5}$$

Likewise, integrating $\partial \mathbf{F}/\partial y$ and $\partial \mathbf{G}/\partial z$ over grid cells results in

$$\overline{\frac{\partial \mathbf{F}}{\partial y}} = \frac{\partial \bar{\mathbf{F}}}{\partial y} - \frac{\partial h_x}{\partial y}\mathcal{O}(h_x) - \frac{\partial h_y}{\partial y}\mathcal{O}(h_y) - \frac{\partial h_z}{\partial y}\mathcal{O}(h_z) \tag{A.6}$$

and

$$\overline{\frac{\partial \mathbf{G}}{\partial z}} = \frac{\partial \bar{\mathbf{G}}}{\partial z} - \frac{\partial h_x}{\partial z}\mathcal{O}(h_x) - \frac{\partial h_y}{\partial z}\mathcal{O}(h_y) - \frac{\partial h_z}{\partial z}\mathcal{O}(h_z). \tag{A.7}$$

The large eddy equations thus become (summing on i)

$$\frac{\partial \bar{\mathbf{U}}}{\partial t} + \frac{\partial \bar{\mathbf{E}}}{\partial x} + \frac{\partial \bar{\mathbf{F}}}{\partial y} + \frac{\partial \bar{\mathbf{G}}}{\partial z} = \frac{\partial h_i}{\partial t}\mathcal{O}(h_i) + \frac{\partial h_i}{\partial x}\mathcal{O}(h_i) + \frac{\partial h_i}{\partial y}\mathcal{O}(h_i) + \frac{\partial h_i}{\partial z}\mathcal{O}(h_i). \tag{A.8}$$

From (A.8) it is clear that changes in grid spacing give rise to unknown second-order source terms in the governing equations. This has strong implications for simulations on nonuniform grids where the flow contains unresolved scales of motion. If grid distortions are large, then the spatial derivatives on the right-hand side of (A.8) will contaminate the solution. Additionally, if sudden changes are made to the grid during the course of a simulation (e.g., a remap in an arbitrary Lagrangian Eulerian (ALE) calculation), then the temporal derivatives on the right-hand side of (A.8) will corrupt the results.

In the preceding derivation, the trapezoidal rule was used, in reverse, in order to regain certain integrals and thus obtain the large eddy equations in the same form as the N–S equations. This procedure gave rise to the $\mathcal{O}(h_\xi)$ terms in (A.3), (A.5), (A.6), and (A.7). The exact expression for the error associated with the Trapezoidal rule is

$$\epsilon^T \equiv \int_{\xi - h_\xi/2}^{\xi + h_\xi/2} \phi(\xi')\, d\xi' - h_\xi \left(\frac{\phi(\xi - h_\xi/2) + \phi(\xi + h_\xi/2)}{2} \right) = -\frac{h_\xi^3}{12}\frac{\partial^2 \phi(\eta)}{\partial \eta^2} \tag{A.9}$$

for some $\eta \in (\xi - h_\xi/2, \xi + h_\xi/2)$. The error vanishes for functions which are linear over the region of integration, i.e., for $\partial^2\phi(\eta)/\partial\eta^2 = 0$. Therefore, if grid irregularities are restricted to laminar regions of the flow, then the right-hand side of (A.8) will be negligible (assuming the flow is well-resolved in such regions).

ACKNOWLEDGMENTS

The author thanks Dr. J. A. Greenough, Dr. A. Kuhl, and Dr. O. Schilling for helpful suggestions concerning the manuscript, Dr. T. S. Carman for proofreading the Appendix, Dr. P. G. Dykema and Dr. J. H. Bolstad for numerical advice, and Professor. J. A. Domaradzki for informative discussions regarding filtering.

REFERENCES

1. D. A. Anderson, J. C. Tannehill, and R. H. Pletcher, *Computational Fluid Mechanics and Heat Transfer* (Hemisphere, Washington, DC/New York, 1984).

2. J. B. Bell, M. J. Berger, J. S. Saltzman, and M. Welcome, Three-dimensional adaptive mesh refinement for hyperbolic conservation laws, *SIAM J. Sci. Comput.* **15**, 127 (1994).
3. M. J. Berger and P. Colella, Local adaptive mesh refinement for shock hydrodynamics, *J. Comput. Phys.* **82**, 64 (1989).
4. M. J. Berger and J. Oliger, Adaptive mesh refinement for hyperbolic partial differential equations, *J. Comput. Phys.* **53**, 484 (1984).
5. J. A. Domaradzki and K.-C. Loh, The subgrid-scale estimation model in the physical space representation, *Phys. Fluids* **11**, 2330 (1999).
6. J. A. Domaradzki and E. M. Saiki, A subgrid-scale model based on the estimation of unresolved scales of turbulence, *Phys. Fluids* **9**, 2148 (1997).
7. C. Fureby and G. Tabor, Mathematical and physical constraints on large-eddy simulations, *Theoret. Comput. Fluid Dynam.* **9**, 85 (1997).
8. S. Ghosal and P. Moin, The basic equations for the large eddy simulation of turbulent flows in complex geometry, *J. Comput. Phys.* **118**, 24 (1995).
9. H. van der Ven, A family of large eddy simulation (LES) filters with nonuniform filter widths, *Phys. Fluids* **7**, 1171 (1995).
10. O. V. Vasilyev, T. S. Lund, and P. Moin, A general class of commutative filters for LES in complex geometries, *J. Comput. Phys.* **146**, 105 (1998).